Article

Not peer-reviewed version

Mitochondrial sAC-cAMP-PKA Axis Modulates the $\Delta\psi_m$-Dependent Control Coefficients of the Respiratory Chain Complexes: Evidence of Respirasome Plasticity

Rosella Scrima *, Olga Cela, Michela Rosiello, Ari Qadir Nabi, Claudia Piccoli, Giuseppe Capitanio, Francesco Antonio Tucci, Aldo Leone, Giovanni Quarato, Nazzareno Capitanio *

Posted Date: 30 September 2023

doi: 10.20944/preprints202309.2144.v1

Keywords: mitochondrial respiratory chain complexes; supercomplexes; cAMP/PKA signaling pathway; soluble adenylate cyclase; metabolic flux theory; mitochondrial membrane potential

Article

Mitochondrial sAC-cAMP-PKA Axis Modulates the $\Delta\Psi_m$-Dependent Control Coefficients of the Respiratory Chain Complexes: Evidence of Respirasome Plasticity

Rosella Scrima [1,*], Olga Cela [1], Michela Rosiello [1], Ari Qadir Nabi [1,2], Claudia Piccoli [1], Giuseppe Capitanio [3], Francesco Tucci [4], Aldo Leone [1], Giovanni Quarato [5] and Nazzareno Capitanio [1,*]

[1] Department of Clinical and Experimental Medicine, University of Foggia, Foggia 71122, Italy
[2] Department of Biology, College of Science, Salahaddin University-Erbil, Erbil, 44001, Kurdistan, Iraq.
[3] Department of Translational Biomedicine and Neuroscience, University of Bari "Aldo Moro", 70124 Bari, Italy
[4] European Institute of Oncology IRCCS, 20141, Milan, Italy
[5] Treeline Biosciences, San Diego, CA 92121, USA
* Correspondence: rosella.scrima@unifg.it; nazzareno.capitanio@unifg.it

Abstract: The current view of the mitochondrial respiratory chain complexes I, III and IV foresees the occurrence of their assembly in supercomplexes providing additional functional properties as compared with randomly colliding isolated complexes. According to the plasticity model the two structural states of the respiratory chain may interconvert influenced by the intracellular prevailing conditions and in previous studies we candidated the mitochondrial membrane potential as a factor controlling their dynamic balance. Here, we investigated if and how the cAMP/PKA-mediated signalling influences the aggregation state of the respiratory complexes. Analysis of inhibitory-titration profiles of the endogenous oxygen consumption rates in intact HepG2 cells with specific inhibitors of the respiratory complexes was performed to quantify, in the framework of the metabolic flux theory, the corresponding control coefficients. The results attained inhibiting pharmacologically either PKA or sAC indicate that the reversible phosphorylation of the respiratory chain complexes/supercomplexes influences their assembly state in response to the membrane potential. This conclusion is supported by scrutiny of the available structure of the CI/$CIII_2$/CIV respirasome enabling to map several PKA-target serine residues exposed to the matrix side of the complexes I, III and IV at the contact interfaces of the three complexes.

Keywords: mitochondrial respiratory chain complexes; supercomplexes; cAMP/PKA signaling pathway; soluble adenylate cyclase; metabolic flux theory; mitochondrial membrane potential

1. Introduction

The mitochondrial respiratory chain is constituted by inner membrane-embedded respiratory complexes (RCs) (CI, NADH dehydrogenase; CII, succinate dehydrogenase; CIII, Cytochrome c reductase/bc1; CIV, cytochrome c oxidase) sequentially transferring reducing equivalents to dioxygen, which is reduced to H_2O [1]. Part of the redox energy, thus made available, is harnessed by CI, CIII and CIV to pump protons from the matrix side to the intermembrane space thereby establishing an electrochemical proton gradient largely constituted by the electrical component $\Delta\Psi_m$ [2] The protonmotive force is, henceforth, utilized to drive endergonic reactions mainly the ATP synthesis by the H^+-F_oF_1-ATP synthase (CV).

The long-standing view of the RCs as independent entities functionally connected by the freely diffusible CoQ and cytochrome c as mobile redox carriers (fluid model) [3] has been disputed in the last two decades by the emerged evidence that the mitochondrial respiratory chain complexes interact each other forming stable supercomplex (SC) assemblies with defined stoichiometric ratios

(solid model) [4]. However, neither model satisfactorily account for conflicting experimental evidence and the discrepancies are not yet solved [5,6]. The *in-situ* identification of the fraction of the RCs organized in SCs is a challenging task and the occurrence of artifacts in the ex-situ experimental procedures cannot be ruled out.

An alternative model foresees a balanced distribution between free RCs and SCs with the two pools in a dynamic equilibrium (plastic model) [7-9]. This opens the issue to the possibility that the balance between RCs vs SCs might be controlled by physiological/metabolic cues [10].

An alternative to tackle the controversy is to make use of a functional approach. The flux control theory is a mathematical framework that enables to model the contribution of distinct enzymatic steps to the overall metabolic flux pursued by the pathway wherein those steps are components [11-13]. Each step can be graded with a specific control coefficient ranging theoretically from 0 to 1 if its strength in controlling the overall flux varies from a negligible to an absolute contribution respectively. The control coefficient of a specific step can be assessed experimentally by comparing the activity of the overall flux with that of the isolated selected step both titrated independently with the same concentrations of a specific inhibitor of the enzymatic step. The "summation corollary" of the theory foresees that the sum of the control coefficients of all the steps contributing to the pathway must closely approach the unity [11,12]. If the sum of the control coefficients is higher than the unity this means that two or more enzymatic steps works in a functional complex (see Supplemental Figure S1).

Identification of the enzymatic step(s) kinetically controlling the overall respiratory flux and, consequently, the oxidative phosphorylation (OxPhos) has been the object of extensive investigations within the framework of the "metabolic flux control theory" [14-16]. The ensued results, however, provided inhomogeneous outcomes. The reasons of the discrepancies proved to relay on: i) the integrity of the biological sample utilized; ii) the choice of the respiratory substrate(s); iii) the energetic state of the mitochondrial membrane.

On this basis in previous studies in intact cells we reported that the sum of the control coefficients of the mitochondrial RCs significantly exceeded the unity value when the oxygen consumption rate was titrated with inhibitors of either one of CxI, CxII, CxIII, CxIV under uncoupled condition (i.e. in the presence of FCCP or valinomycin) or conditions utilizing the membrane potential ($\Delta\Psi_m$) (i.e. state III of respiration). Conversely under conditions preserving the $\Delta\Psi_m$ (i.e. state IV of respiration or in the presence of the CV inhibitor oligomycin) the sum of CI-CIV control coefficients was below one [17,18]. Our interpretation was that the energy state of the mitochondrial inner membrane influences the formation of the SCs from a pool of isolated complexes. In particular, collapse of the $\Delta\Psi_m$ promotes the assembly of CxI, CxIII and CxIV. This might be envisioned as an adaptive response of the OxPhos system to the cellular bioenergetics demand with enhancement of the $\Delta\Psi_m$ taken as a signal of low protonmotive force-consuming F_oF_1-ATP-synthase activity. Under this condition supercomplexes would dis-assemble in their RCs constituent thereby slowing-dawn respiration and sparing reducing substrates. The opposite would occur if the protonmotive force is utilized (with substantial reduction of the $\Delta\Psi_m$ for ATP synthesis). In this case formation of respirasomes is favoured with enhanced respiration to fulfil the greater energy needs.

Post-translational modification of proteins plays a well-recognized and amply documented important role for rapid and transient changes in the structure of a protein modulating enzyme activity as well as interfering or favouring protein-protein interactions. Recent extensive proteomic analysis has revealed a previously unexpected and wide range of post-translational modification of the mitochondrial proteome including all the components of the OxPhos machinery [19]. Reversible phosphorylation of practically all the RCs has been reported to be the most common covalent modification [20-22] consistent with the presence in mitochondria of kinases and phosphatases for both serine/threonine and tyrosine residues [23,24]. However, although, a large body of evidence is available about the functional impact of phosphorylation/dephosphorylation of individual RCs (some time conflicting) to the best of our knowledge only a few reports have directly or indirectly investigated the role of post-translational modifications in SC assembly and function.

 doi:10.20944/preprints202309.2144.v1

In the present study we have extended our previous observations and carried out a systematic analysis on inhibitory-titration curves to investigate the impact of the cAMP/PKA signalling cascade on the distribution of the flux control coefficients among the protonmotive RCs and the influence on this of the membrane energy state.

2. Results

2.1. The respiratory flux control coefficient of CIV is influenced by the mitochondrial respiratory state and by the activity of PKA.

Intact HepG2 cells were grown in the presence of calf serum and assayed for endogenous mitochondrial respiratory activity by high resolution respirometry (Figure 1A,B). Two conditions were selected, resting and FCCP-uncoupled respiration. As compared with the resting condition the presence of the protonophore FCCP resulted in a 2-fold increase in the oxygen consumption rate (OCR) and complete collapse of the $\Delta\Psi_m$ (see ahead Figure 3 A,B). The oxygen consumption rates under both conditions (OCR_{Rest} and OCR_{Unc}) were titrated with increasing concentrations of the cytochrome c oxidase-inhibitor KCN. As shown in Figure 1B normalized OCR_{Rest} and OCR_{Unc} resulted in different inhibitor-titration profiles, particularly evident at the lower KCN concentrations, with the OCR_{Rest} resulting significantly more resistant to KCN inhibition as compared with the OCR_{Unc}. The difference can be better visualized in a plot correlating the percentages of activities attained for the resting and uncoupled respiration at the same concentration of KCN (Figure 1C). The results shown confirm what already reported [17,18] but serve as internal control for the other conditions tested throughout the present study.

To investigate if the PKA-mediated signalling pathway, likely activated by continuous exposure of HepG2 cells to serum, had some effect on their respiratory activities we carried out the above-described titration assay with HepG2 cells pre-treated with the PKA inhibitor H89 (Figure 1D). The results obtained and illustrated in Figure 1 E,F show that H89 treatment abolished the differences in the KCN-titration profiles when the coupled and uncoupled OCRs were compared with the OCR_{Rest} losing its apparent more resistance to KCN. Accordingly, the graph correlating OCR_{Rest} and OCR_{Unc} resulted in data points lying on the diagram diagonal (Figure 1F). To note, when HepG2 cells were treated with the phosphodiesterase (PDE) inhibitor IBMX (Figure 1G) the KCN-titration profiles under respiratory coupled and uncoupled conditions resembled what observed with the untreated control cells (Figure 1 H,I).

The specific inhibitory profile of an enzymatic step that is part of a measured metabolic flux can be exploited to assess the relative contribution of that step in controlling the flux [25]. On this basis we thought to quantify the respiratory flux control coefficients of complex IV ($C^{J}_{v,CIV}$). To this aim the inhibitory-titration data sets reported were subjected to non-linear regression analysis as developed in [25,26] and modified in [18]. From the best fits a $C^{J}_{v,CIV}$ of 0.08 ±0.02 and of 0.81 ±0.08 was obtained for the OCR_{Rest} and OCR_{Unc} respectively in untreated HepG2 cells. Treatment with H89 resulted in $C^{J}_{v,CIV}$ of 0.79 ±0.08 and of 0.75 ±0.06 for the OCR_{Rest} and OCR_{Unc} respectively whereas it was 0.15 ±0.04 for OCR_{Rest} and 0.85 ±0.06 for OCR_{Unc} in IBMX-treated cells. The difference of the $C^{J}_{v,CIV}$ under OCR_{Rest} between untreated and H89-treated cells was statistically highly significant as well as between OCR_{Rest} and OCR_{Unc} in untreated and IBMX-treated cells, but not in H89-treated cells.

Preprints (www.preprints.org) | NOT PEER-REVIEWED | Posted: 30 September 2023 doi:10.20944/preprints202309.2144.v1

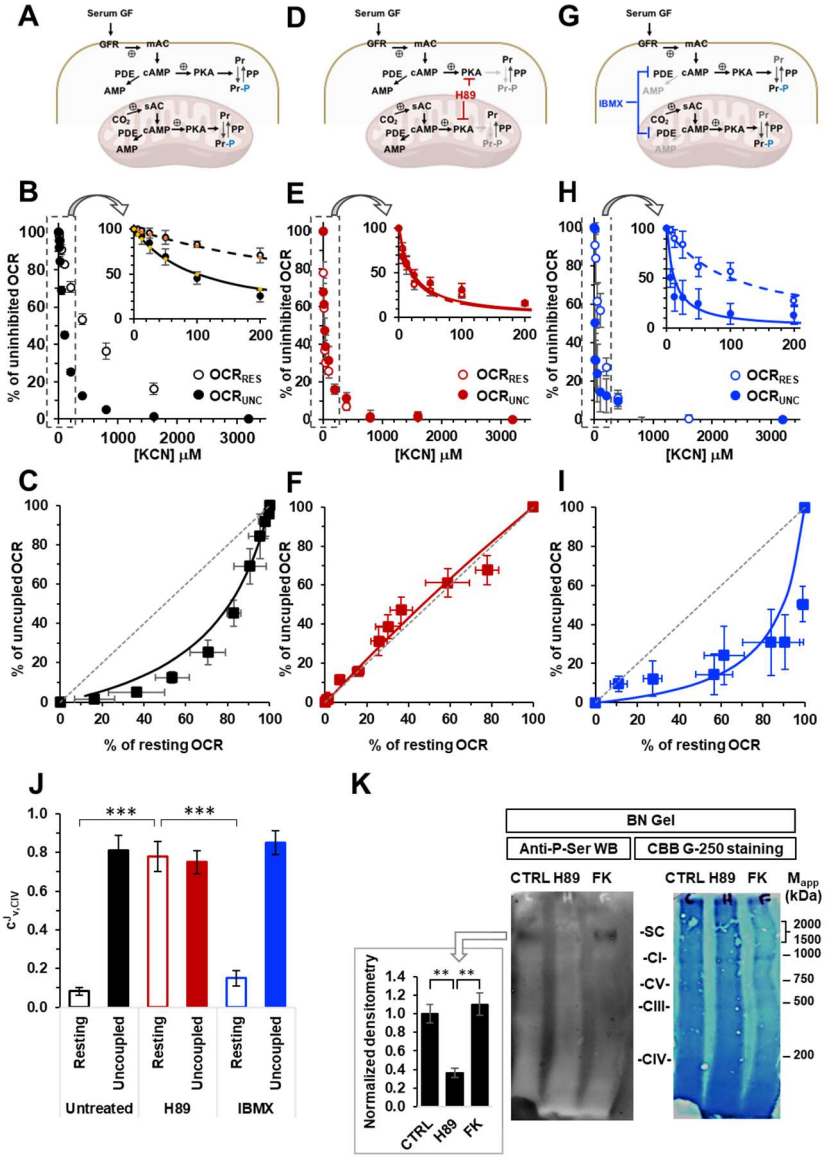

Figure 1. Effect of modulators of the cAMP-PKA signalling axis on the KCN inhibitory titrations of the mitochondrial respiratory activity in intact HepG2 cells. (A), (D) and (G) show schematically the signalling pathway object of the investigation under untreated condition (A) and in the presence of H89 (D) or IBMX (G); GF, growth factors; GFR, growth factor receptor; mAC, membrane adelylate cyclase; PDE, phosphodiesterase; PKA, protein kinase A; PP, protein phosphatase; Pr, proteins; Pr-P, phosphorylated proteins; sAC, soluble adelylate cyclase. Endogenous substrates-sustained respiration in HepG2 cells was assayed by high resolution oxymetry in the absence or presence of 1 µM FCCP as detailed in Materials and Methods. The oxygen consumption rates were measured after the addition of about 2 x 10^6 cells/ml and titrated with increasing concentrations of KCN. The oxygen consumption rates (OCRs) are shown as percentage of the uninhibited OCR at the concentrations of KCN tested in untreated (B, C), H89-treated (0.5 µM x 2 hours) (E, F) and IBMX-treated (100 µM x 2 hours) (H, I) cells. In (B, E, H) the activity is shown under resting condition (OCR_{RES} empty symbols) and under uncoupled conditions (OCR_{UNC}, filled symbols) as mean values ± SEM of 5-7 independent biological replicates under each condition; the insets detail the titration curves at relatively low and intermediate concentrations of KCN with the dashed and continuous lines showing the best fitting according to the equation described in Materials and Methods. (C), (F) and (I) are plots of the OCR_{RES} vs OCR_{UNC} measured at the same concentrations of KCN with the continuous lines resulting from combination of those fitting the corresponding titration curves and the dotted thin line indicating the diagonal of the diagram. (J) Histogram showing the flux control coefficient ($c^J_{v,CIV}$) of complex IV on

 doi:10.20944/preprints202309.2144.v1

the respiratory activity under resting and uncoupled conditions in untreated and H89- and IBMX-treated cells; the values are means ± SEM of the parameter computed from best-fitting the single titration curves averaged in B, E and H; ***, $p < 0.001$. (K) Representative immunoblotting with anti-P-serine of mitochondrial extracted proteins separated by BN-native gel electrophoresis (shown on the right as stained by coomassie blu brilliant (CBB)-G250) as detailed in Materials and Methods. The histogram shows the densitometric analysis of the immunostained high molecular weight band as means ± SEM of three independent biological replicates under each condition; **, $p < 0.005$ (CTRL, untreated cells; H89-treated cells; FK, forskolin-treated cells).

To verify that the above-described treatment of HepG2 cells with H89 effectively impacted on the cAMP-PKA axis we carried out an immunoblot assay using an anti-P-Ser antibody on mitoplast-extracted proteins under native conditions in the presence of an amount of dodecyl maltoside reported to preserve the quaternary structure of all the RCs as well as their sovramolecular aggregations [27]. Figure 1K shows a representative anti-P-ser immunoblot for untreated and H89-treated HepG2 samples compared with the parental Coomassie Blue stained gel. A clear stained anti-P-ser band can be observed in the untreated sample with an apparent molecular weight exceeding those of the RCs as shown by comparison with the Coomassie blue stained gel. Notably, in the H89-treated sample this band was markedly dampened whereas it was present in sample from HepG2 cells treated with the adenylate cyclase-activating compound forskolin, with a staining intensity comparable with that of the untreated sample.

2.2. Inhibition of the soluble adenylate cyclase affects the respiratory flux control coefficients of CI, CIII and CIV under resting respiratory state.

Several isoforms of PKA have been described with distinct intracellular compartmentalization [28] and mitochondria-localized PKA have also been reported but with the second messenger cAMP formed by a soluble HCO_3^--dependent adelylate cyclase (sAC) [29,30]. Being sAC specifically inhibitable by KH7 [31] we decided to replicate the inhibitory-titration assay shown in Figure 1 but with HepG2 cells treated with KH7 (Figure 2 A,B). Moreover, we extended our analysis to complex I and to complex III using rotenone and myxothiazol as specific inhibitors, respectively. The results of this systematic analysis are shown in Figure 2.

Figure 2C shows once again the KCN-related inhibitory profiles of the OCR_{Res} and OCR_{Unc} in untreated control cells. The results attained confirm what already shown in Figure 1B but are needed because used as internal control in a cohort of experiments carried out in a temporally distinct phase of this study. As for the results attained with H89-treated cells also in KH7-treated cells the difference in the inhibitory profiles of OCR under resting and uncoupled conditions was practically abolished (Figure 2 D) and confirmed in the OCR_{Res} vs OCR_{Unc} plot (Figure 2 E). When the OCR was titrated with the complex I inhibitor rotenone the inhibitory-titration profiles under coupled and uncoupled conditions closely resembled qualitatively what attained following KCN-titration in untreated sample (Figure 2 F). Most notably, treatment with KH7 resulted in similar inhibitory profiles irrespective of the respiratory state (Figure 2 G,H). A behaviour similar to what observed for the inhibitory-titration curves with KCN and rotenone was recapitulated in cells titrated with the complex III inhibitor myxothiazol (Figure 2 I,J,K).

2.3. The sum of the respiratory flux control coefficients of CI, CIII and CIV indicates the occurrence of supercomplexes in uncoupled respiration and in the presence of inhibitors of the cAMP/PKA signaling pathway.

Applying the fitting procedure to the titration curves shown in Figure 2 enabled to estimate the respiratory flux control coefficients of complexes IV ($c^J_{v,CIV}$), I ($c^J_{v,CI}$) and III ($c^J_{v,CIII}$). As shown in Figure 3A in untreated cells the control coefficients estimated under resting respiration was significantly lower than those measured under uncoupled condition for all the RCs ($c^J_{v,CIV}$: 0.30 ± 0.10 *vs* 0.75 ± 0.07; $c^J_{v,CI}$: 0.19 ± 0.09 *vs* 0.70 ± 0.15; $c^J_{v,CIII}$: 0.39 ± 0.08 *vs* 0.95 ± 0.04). Conversely, treatment with KH7 resulted in relatively large control coefficients for all the RCs and irrespectively from the mitochondrial

Preprints (www.preprints.org) | NOT PEER-REVIEWED | Posted: 30 September 2023 doi:10.20944/preprints202309.2144.v1

membrane energy state ($cJ_{v,CIV}$: 0.90 ± 0.05 *vs* 0.90 ± 0.08; $cJ_{v,CI}$: 0.72 ± 0.17 *vs* 0.75 ± 0.04; $cJ_{v,CIII}$: 0.70 ± 0.12 *vs* 0.70 ± 0.15). Most importantly, when the control coefficients of complexes I, III and IV were summed up in the different conditions tested it resulted that the sum was close to the unity under resting respiration in untreated cells whereas it was largely exceeding the unity (i.e. > 2) in uncoupled untreated cells as well as in KH7-treated cells irrespective of the respiration state (Figure 3B).

Figure 3C shows the effect of the drugs targeting the PKA-mediated signaling, tested in this study, on the uninhibited OCRs. While in untreated and IBMX-treated cells the maximal OCR_{Unc} was, as expected, higher than the OCR_{Rest} in both the H89- and KH7-treated cells the OCR_{Unc} was significantly inhibited as compared with that in untreated cells. On the contrary, no significant differences were observed in untreated and drug-treated cells as far as the OCR_{Res} was concerning. Consequently, the respiratory reserve capacity (i.e. the difference between OCR_{Unc} and OCR_{Res}), present in untreated and IBMX-treated HepG2 cells, was practically zeroed in H89- and KH7-treated samples.

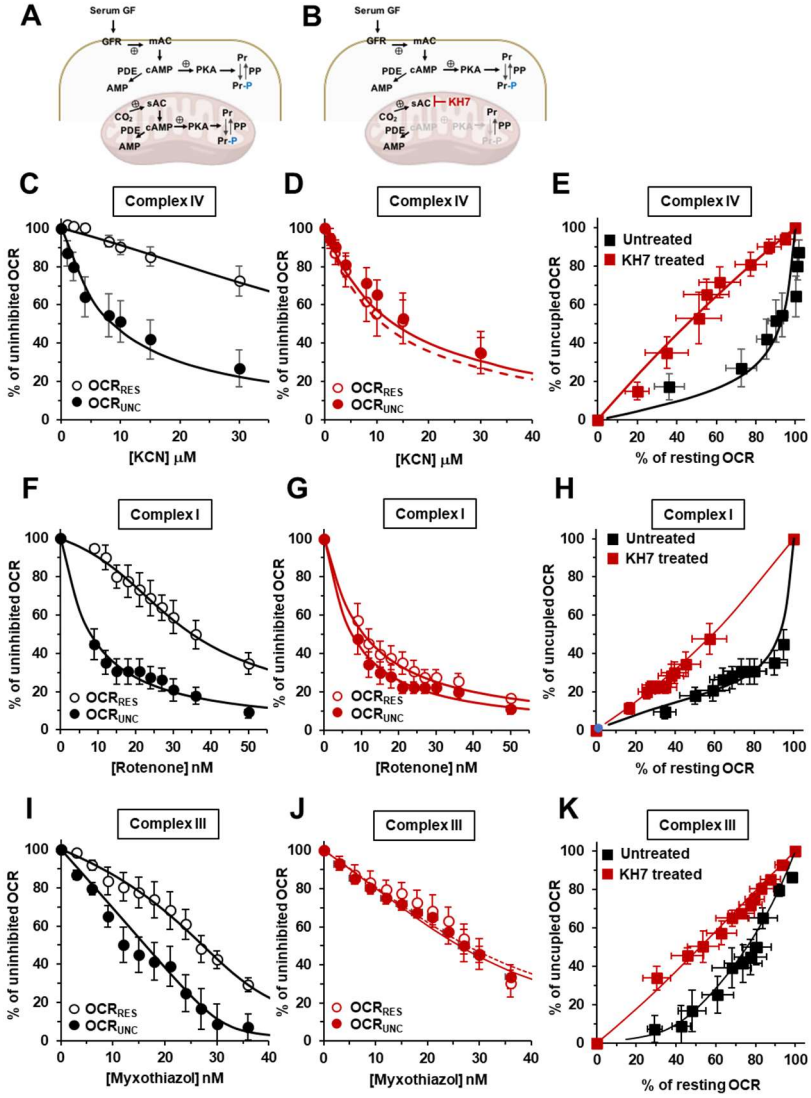

Figure 2. Effect of the inhibition of sAC by KH7 on the KCN, rotenone and myxothiazol inhibitory titrations of the mitochondrial respiratory activity in intact HepG2 cells. (A) and (B) show schematically the signalling pathway object of the investigation under untreated condition (A) and in the presence of KH7 (B); see legend to Figure 1 for definition of the abbreviations. Endogenous substrates-sustained respiration in HepG2 cells was assayed by high resolution oxymetry in the absence or presence of 1 µM FCCP as detailed in Materials and Methods. The oxygen consumption rates (OCRs) were measure after the addition of about 2 x 10^6 cells/ml and titrated with increasing concentrations of either one of KCN, rotenone, myxothiazol. The OCRs are shown as percentage of

Preprints (www.preprints.org) | NOT PEER-REVIEWED | Posted: 30 September 2023 doi:10.20944/preprints202309.2144.v1

the uninhibited OCR at the relatively low and intermediate concentrations of KCN (C), rotenone (F) and myxoyhiazol (I) in untreated cells and in KH7-treated cells (25 μM x 2 hours) (D, G, J respectively); the activity is shown under resting condition (OCR_{Res} empty symbols) and under uncoupled conditions (OCR_{Unc}, filled symbols) as mean values ± SEM of 5-7 independent biological replicates under each condition with the dashed and continuous lines showing the best fitting according to the equation described in Materials and Methods. (E), (H) and (K) are plots of the OCR_{RES} vs OCR_{Unc} measured at the same concentrations of KCN, rotenone and myxothiazol respectively with the continuous lines resulting from combination of those fitting the corresponding titration curves. .

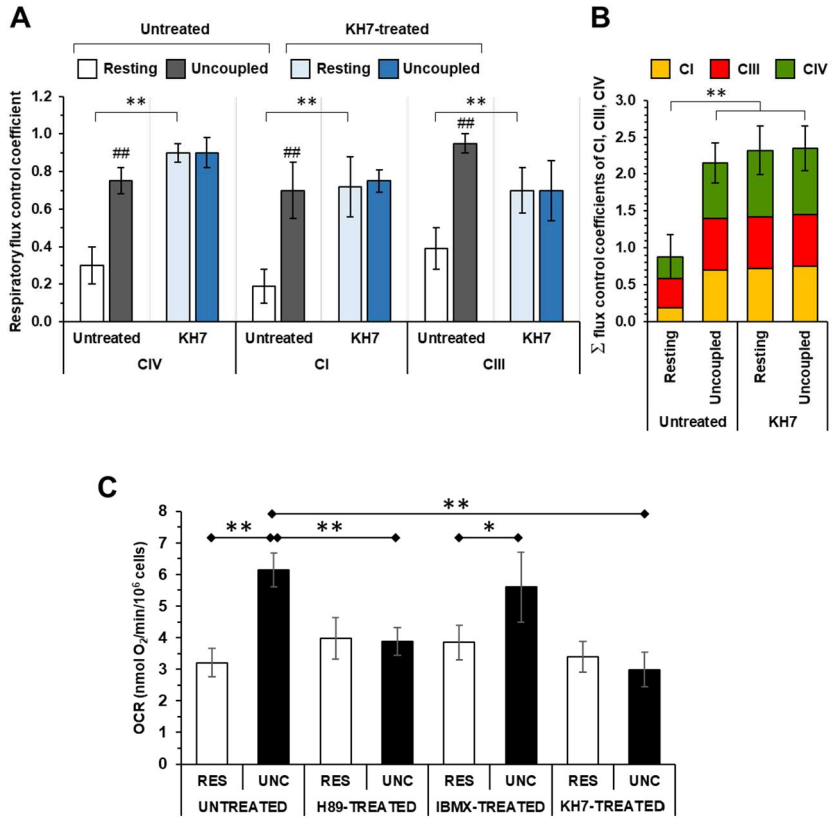

Figure 3. Effect of sAC inhibition on the respiratory flux control coefficients of CI, CIII, CIV and of the cAMP-PKA modulation on the uninhibited oxygen consumption rate in HepG2 cells. (A) respiratory flux control coefficients of CIV, CI and CIII under resting and uncoupled condition as computed from the inhibitory titration curves shown in Figure 2 C,F,I for untreated and in Figure 2 D,G,J for KH7-treated cells. The values are means ± SEM of the parameter computed from best-fitting the single titration curves (n=5-7) averaged in Figure 2; **, $p < 0.01$. (B) Histogram showing the sum of the control coefficients of CI, CIII and CIV under uncoupled and coupled respiration in untreated and KH7-treated cells. (C) Histogram showing the effect of H89, IBMX and KH7 treatment on the oxygen consumption rates (OCR) in cells under resting (RES) and uncoupled (UNC) respiratory conditions. OCR was measured polarographically as detailed under Materials and Methods and the bars are means ± SEM of 7-10 independent biological replicates under each conditions; *, $P < 0.05$; **, $P < 0.01$.

2.4. Inhibition of the cAMP/PKA axis does not affect the respiration-driven mitochondrial membrane potential generation.

To verify if the observed inhibitory effect on the maximal activity of cells following H89 or KH7 treatments was also accompanied to an uncoupled effect under resting condition we measured the mitochondrial membrane potential ($\Delta\psi_m$) under resting respiration. To this aim HepG2 cell membranes were permeabilized with digitonin (Figure 4A) supplemented with NADH-linked

Preprints (www.preprints.org) | NOT PEER-REVIEWED | Posted: 30 September 2023 doi:10.20944/preprints202309.2144.v1

respiratory substrates and the $\Delta\psi_m$ estimated from the fluorescence quenching of safranine. As shown in Figure 4B both untreated and KH7-treated respiring HepG2 cells caused quenching of the safranine-related fluorescence to a similar extent that was completely recovered following addition of the uncoupler FCCP. From this outcome the $\Delta\psi_m$ was quantified and resulted to be around 130 mV both in untreated and KH7-treated cells. This result ruled out that the inhibitory-titration profiles observed under resting (i.e. coupled) conditions in H89 and KH7-treated cells and mimicking what attained in the presence of FCCP, was trivially due to an uncoupling effect caused by the drug treatment.

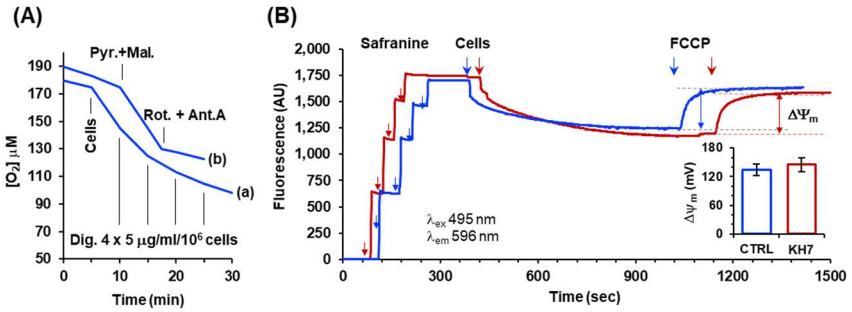

Figure 4. Measurement of respiration-driven mitochondrial membrane potential in permeabilized HepG2 cells. (**A**) Representative oxymetric traces showing the protocol utilized to permeabilize plasma membrane in HepG2 cells. Trace (a): 2 x 10^6 cells/ml were added to the assay buffer (detailed under Material and Methods) and supplemented as indicated with consecutive additions of digitonin (Dig); trace (b) 2 x 10^6 cells/ml were pre-incubated with 15 µg/ml/10^6 cells of digitonin were suspended in the assay buffer and supplemented, where indicated, with 2 µM pyruvate plus 2 µM malate followed by injection of 2 mM rotenone plus 1 mM antimycin A. (**B**) Representative spectrophotometric traces for assessment of the mitochondrial membrane potential ($\Delta\Psi_m$) in untreated (blue line) and KH7-treated (red line) cells. Where indicated the assay buffer supplemented with pyruvate and malate was injected with four consecutive additions of 2.5 µM safranine O followed by addition of previously digitonin-permeabilized cells (2x10^6/ml); after stabilization of the quenched fluorescence 0.5 µM FCCP was added. The fluorescence difference recorded before and after addition of FCCP is a measure or the respiration-driven $\Delta\Psi_m$ generation; the histogram in the inset shows quantification in mV of the $\Delta\Psi$m, as described in Materials and Methods, with the bars means ± SEM of 4 independent biological replicates.

2.5. A number of PKA-target serine residues are present at the contact sites of CI, CIII and CIV in the supercomplex.

Given the availability of several cryo-EM-resolved atomic structures of the respiratory chain SC we decided to map on it the positions of PKA-targetable residues. Figure 5 A shows the porcine SC that is currently the structure with the highest resolution (pdb 5GUP, 4.0 Å) [32]. The SC is constituted by one unit of complex I interacting with a complex III dimer and a complex IV monomer (i.e. CI,$CIII_2$,CIV). Exploiting the outcome of an extensive phospho-proteome bioinformatic analysis pinpointing in RCs all the residues target of known serine/threonine/tyrosine protein kinases [20], we unbiasedly mapped the positions of only those targetable by PKA in the SC structure. Surprisingly, many of the PKA targetable serine/threonine residues located at the interfaces of the complexes and most notably at contact sites between CI-CIII, CIII-CIV and CIV-CI and potentially accessible from the matrix side of the membrane (Figure 5B). Interestingly, some of these residues are proximal to salt bridges connecting CI and CIV (i.e. Ser14 in subunit 7C of CIV close to salt bridge formed between Arg20 in subunit 7C of CIV and Glu503 in subunit ND5 of CI) and to contact points linking CI to CIII (i.e. Ser26 of subunit NDUFB4/B15 of CI close to Glu258, Glut259, Asp260 in Core I of CIII). Notably, with this latter recently reported to be essential for respirasome stabilization [33].

Preprints (www.preprints.org) | NOT PEER-REVIEWED | Posted: 30 September 2023 doi:10.20944/preprints202309.2144.v1

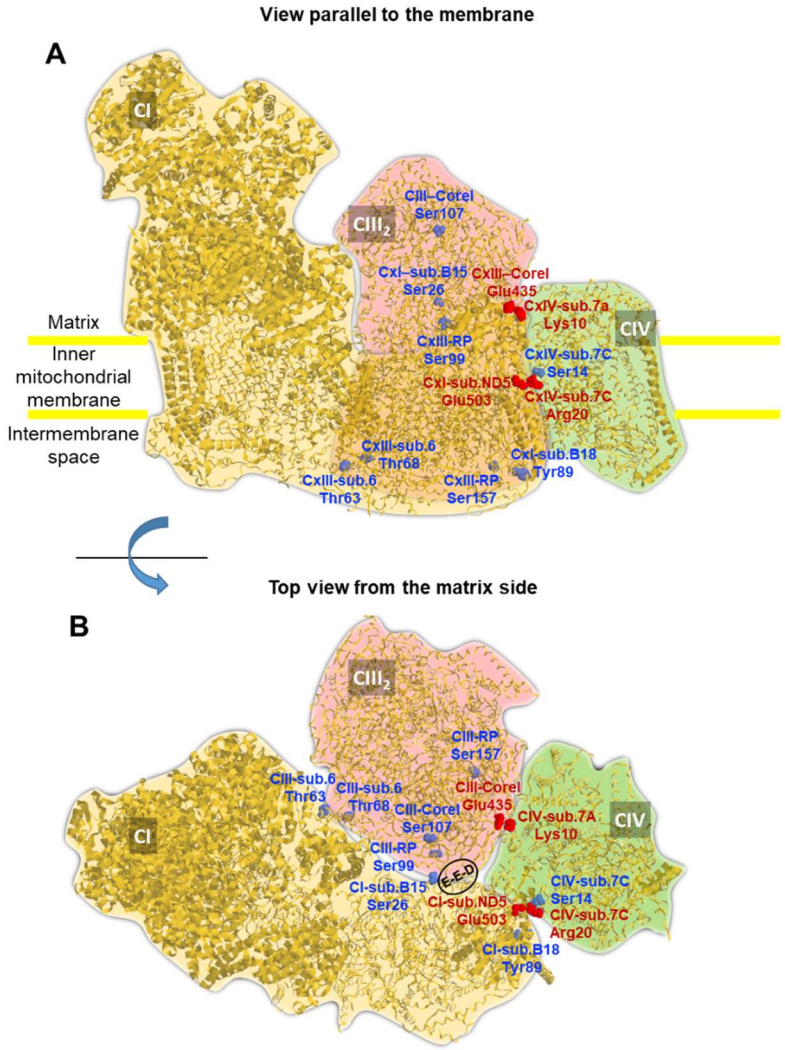

Figure 5. Structure of the mitochondrial respirasome with localization of PKA-targetable residues. The cryo-EM-derived structure of the mitochondrial respiratory SC CI/CIII2/CIV from *Sus scrofa* is shown (pdb code 5GUP). The silhouette of the individual complexes is highlighted with different colours and the view parallel to the membrane (**A**) and the top view from the matrix side (**B**) are shown. Serine and threonine residues target of PKA are pinpointed in the structure (in blue) with indication of the complex-subunit of their location; the numbering of the residues corresponds to the primary sequence of the specific subunit in *Homo sapiens* after alignment to that of the porcine sequence. Two inter-complex salt bridges between complexes I-IV and III-IV are also shown in red. The encircled residues E-E-D indicate Glu258-Glu259-Asp260 in the Core I of CIII. See text for further details. The picture was drawn by RasTop 2.2 (geneinfinity.org/rastop/).

3. Discussion

The notion of a supramolecular organization of the mitochondrial RCs is supported by convincing evidence. Since the first reports identifying aggregations of RCs under native electrophoresis [4] the recent advance in cryo-EM analysis has contributed to assess structural details of the SCs/respirasomes architecture at atomic resolution [32,34]. Several aggregations of the complexes, with defined stoichiometries, have been identified with that containing one unit of complex I, a dimeric complex III and one unit of complex IV (complex II is not present) being the more abundant assembly formulation [27]. Moreover, several biogenetic factors have been identified facilitating the SCs maturation [35].

Acquisition of a supramolecular structure versus isolated units of the respiratory chain would confer additional functional properties such as facilitated electron transfer to the final acceptor O_2.

 doi:10.20944/preprints202309.2144.v1

This would reduce the risk of electron diversion/leak to O_2 with formation of potentially harmful reactive oxygen species [35]. Notably, all the three complexes, I-III-IV, are redox-linked proton pumps, and perhaps the concerted locally generated transmembrane electrochemical potential could also modulate its chemiosmotic coupling with the H^+-F_oF_1-ATP synthase [37].

Nevertheless, SCs coexist with a pool of isolated units of each of the RCs that would constitute a reservoir from where the SC biogenesis taps. There is no reason to consider this pool of isolated complexes not competent in transferring reducing equivalents by a random collision mechanism. This infers the suggestive possibility that the isolated RCs are in a dynamic equilibrium with SCs as indeed foreseen by a proposed "plastic" model of the respiratory chain [7,38]. Importantly, the prevailing metabolic state in the cell as well as the bioenergetic state of the membrane could shift the SCs vs isolated RCs balance to better cope with the actual cellular energetic needs [10,17,18,39].

Proving the occurrence of the above-mentioned balance is experimentally challenging. Indeed, all the current methodological approaches to detect the assembly state of the RCs rely on procedures that destroy the mitochondrial membrane integrity therefore obscuring any functional state of it.

An alternative approach is provided by applying the metabolic flux theory that assesses the specific contribution of individual enzymatic steps in intact cells under controlled different functional states. In the context of the mitochondrial respiratory chain the overall metabolic flux is given by the oxygen consumption rate fuelled by endogenous substrates and the easiest way to determine the individual contribution of the RCs is measuring the impact of their specific inhibition on the respiratory flux [11,12,40]. The summation corollary of the theory foresees that summing up the control coefficients of all the individual enzymatic steps, contributing to a given metabolic flux, cannot exceed the unity value unless two or more individual enzymatic steps assemble in supramolecular units.

In the framework of the metabolic flux analysis our group showed in previous studies that the control coefficients of CI, CIII and CIV were markedly affected by the energy state of the mitochondrial membrane under condition mimicking different metabolic states [17,18]. Applying the above-mentioned summation corollary, we proposed a model thereby in the presence of an established respiration-mediated transmembrane electrochemical potential the RCs are prevalently in form of isolated units whereas under low or absent membrane potential the RCs assembles as respirasomes (see model in Figure 7).

The recent improvement of proteomic analysis of mitochondrial proteins is disclosing a previously unappreciated occurrence of many different post-translational covalent modifications including proteins of the OxPhos system [19,20] confirming and extending previously reported sporadic observations. These findings pave the way to the need to understand the impact of these modification on the structural/functional features of the proteins involved. The reversible phosphorylation of one or the other of the complexes of the OxPhos system is the better documented post-translational modification [20-23].

The present study aimed to verify if reversible covalent modifications had some effect in controlling the proposed balance between SCs and isolated RCs. We focused our attention on phosphorylations mediated by activation of the cAMP-PKA bio-signalling axis. Worth noting, standard protocol of cell culturing foresees the supplementation of serum in the culture media to preserve cell viability. However, the large number of growth factors present in the serum maintain constantly activated several signaling pathways including the cAMP-PKA axis that should be taken into account.

Herein we tested the effect of specific inhibitor of PKA on the mitochondrial respiratory activity of intact HepG2 cells and its impact on the inhibition titration profiles of complex IV using KCN as inhibitor, and two conditions were tested (i.e. under resting phosphorylating condition and under fully uncoupled condition elicited by the protonophore FCCP). The results attained clearly showed that inhibition of the PKA by H89 markedly affected the inhibition profile of complex IV on the resting overall respiratory flux thereby abolishing the differences otherwise observed in the untreated cells under the two functional conditions tested. We ascribed this effect to the dephosphorylation of respiratory chain complexes likely occurring by cellular protein phosphatases once PKA is

Preprints (www.preprints.org) | NOT PEER-REVIEWED | Posted: 30 September 2023 doi:10.20944/preprints202309.2144.v1

inhibited. Interestingly, treatment of cells with the phosphodiesterase inhibitor IBMX, expected to enhance the PKA activation, did not result in significative differences either in the respiratory flux and in the KCN-related inhibitory profiles as compared with the untreated control cell. This confirmed that the composite mixture of factors present in the serum-supplemented culture medium ensures practically maximal up-stream activation of the PKA-related signalling pathway [42,43].

As several isoforms and intracellular compartmentalization of PKA, all inhibitable by H89, have been found, including intramitochondrial PKA [24], we further investigated its possible specific involvement in the findings here reported. To this purpose we exploited the notion that activation of the mitochondrial PKA is dependent on the production of cAMP by sAC a distinct soluble isoform of the cytosolic transmembrane tmAC which is selectively inhibited by KH7 [31]. Although sAC is not exclusively present in mitochondria it has been reported that if bioenergetic readouts are studied the consequences following KH7 treatment relies largely on the mitochondrial rather than the cytosolic sAC inhibition [41]. Treatment of HepG2 cells with KH7 closely resembled what observed with H89 regarding the dampening of the relative resistance to KCN in the inhibitory profile under resting respiration and its superimposition to that under uncoupled respiration. Most notably, a similar result was observed when the analysis was extended to both complex I and III. Quantification of the control coefficients of CI, CIII and CIV on the overall respiratory flux and application of the summation principle enabled us to conclude that: a) under conditions favouring the phosphorylation state of the RCs, these were functioning as isolated units under coupled conditions but as SCs once respiration was uncoupled (a similar behaviour was observed following IBMX treatment); b) treatment with either the PKA inhibitor or the sAC inhibitor caused the RCs to function mainly as SCs also under coupled conditions (see the schematic model presented in Figure 6). Our interpretation of the results attained agrees with a recent report showing that isoproterenol-mediated activation of the cAMP/PKA signaling cascade resulted in enhanced formation of SCs in H9c2 heart myoblast cell line [44].

Treatment with drugs inhibiting the PKA-mediated axis resulted, as reported, in dampening of the maximal respiratory activity. Intriguingly the respiratory activity under coupled phosphorylating condition was apparently unaffected by either treatment with H89 or KH7 therefore resulting in complete abolishment of the respiratory reserve capacity. Of note, KH7 treatment fully preserved the respiration-driven $\Delta\Psi_m$ under coupled conditions. One possible interpretation of this puzzling observation is that under resting condition the OxPhos system compensates the defective respiratory activity utilizing all the reserve available. The so stimulated respiratory activity would result $\Delta\Psi_m$-independent and might be consistent with the proposed shift of the RCs from the isolated random-collisioning state toward the more efficient SC state.

A limitation of this study is that although a much larger H89-sensitive immunoreactivity toward anti-P-serine was shown for high molecular weight SCs we did not identify directly the phosphorylatable residues involved. This will be the object of future investigations. However, exploration of the available cryo-EM structure of the CI,$CIII_2$,CIV respirasome to search for serine/threonine residues reported as target of PKA [20] unveiled that most of them are mapped at the interlocked surfaces of the complexes and at contact sites among them largely exposed to the mitochondrial matrix side. Intriguingly, two phosphorylatable serines (i.e. Ser14 on sub. 7C of CIV and Ser26 on sub. NDUFB4/B15 of CI) are in close proximity to a salt bridge connecting CI to CIV or to a loop carrying three negative residues (i.e. Glu258-Glu259-Asp260) in the CIII-core I subunit recently reported to be essential in the stabilization of the respirasome CI/$CIII_2$/CIV [39].

Preprints (www.preprints.org) | NOT PEER-REVIEWED | Posted: 30 September 2023 doi:10.20944/preprints202309.2144.v1

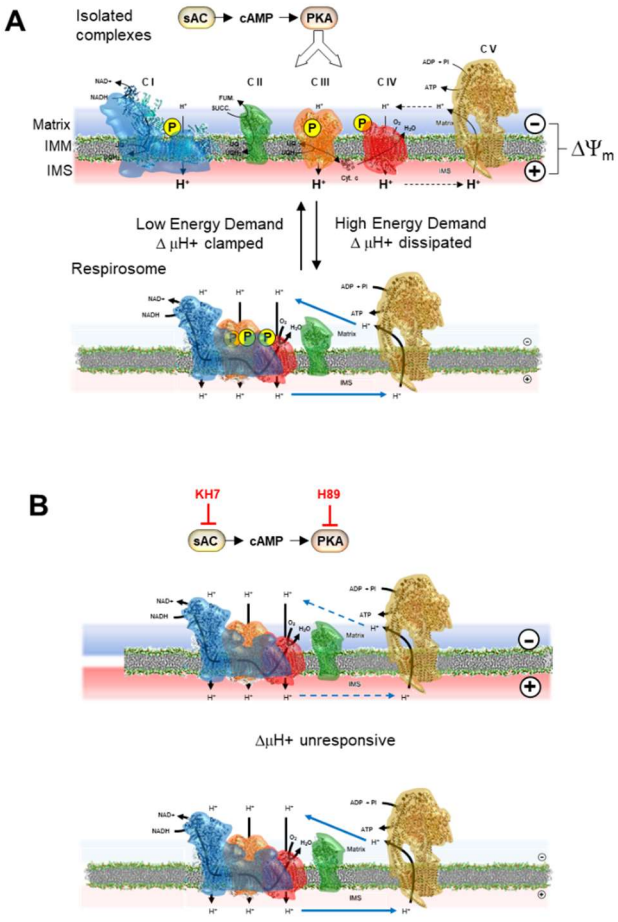

Figure 6. PKA-mediated control of the respiratory chain complexes/supercomplex equilibrium in mitochondrial membrane. Pictorial representation of the model proposed in this study. The respiratory chain complexes are shown in their phosphorylated state under the action of the mitochondrial sAC/cAMP/PKA signaling axis (**A**) as able to change their aggregation state in function of the bioenergetic state of the membrane/metabolic demand with the isolated complexes state favored by the presence of a large electrochemical membrane potential ($\Delta\mu H^+$ largely contributed by $\Delta\Psi_m$) whereas formation of supercomplexes is elicited by low $\Delta\mu H^+$. In (**B**) it is highlighted that the inactivation of the signaling pathway and consequent dephosphorylation of the complexes causes their tendency to form supercomplexes irrespectively of the $\Delta\mu H^+$ extent. IMM, inner mitochondrial membrane; IMS, intermembrane space. See Discussion for further details.

How the $\Delta\Psi_m$ may influence the aggregation state of the RCs can, at the moment, be only object of speculation though computational MD modelling could be insightful. However, well known membrane voltage-sensitive ion channels offer a biophysical prototype demonstrating the impact of the electrical field nearby the membrane surface on the conformational change of membrane-embedded proteins [45,46]. Considering that in respiring mitochondria the electrical component of the proton-motive force has been estimated to reach values of up to 180 mV at the inner mitochondrial membrane [2] (i.e. much larger than that measured at the plasma membrane of excitable cells) it is not surprising that it may exert strong electrostatic interactions with native or post-translationally added charges of protein residues resulting in large conformational changes [47,48].

All together the findings here reported, if confirmed by other more direct approaches, might unveil a hitherto unappreciated level of plasticity and resilience in the mitochondrial OxPhos system.

4. Materials and Methods

4.1. Cell culture.

Preprints (www.preprints.org) | NOT PEER-REVIEWED | Posted: 30 September 2023 doi:10.20944/preprints202309.2144.v1

Human hepatoma-derived cell line (HepG2 from ATCC – HB-8065) was grown in DMEM (Dulbecco's modified Eagle's medium) supplemented with 10% (v/v) foetal bovine serum to 70–80% confluence before harvesting. Drugs treatments: 2 hours with either one of 0.5 µM N-[2-((*p*-Bromocinnamyl)amino)ethyl]-5-isoquinolinesulfonamide (H89), 25 µM (E)-2-(1H-Benzo[d]imidazol-2-ylthio)-N′-(5-bromo-2-hydroxybenzylidene)propanehydrazide (KH7), 100 µM 3-Isobutyl-1-methylxanthine (IBMX), 10 µM Forskolin (FK); after incubation cells were detached from 150 mm-diameter Petri dishes with 2 ml of 0.05% trypsin/0.02% EDTA and washed in 20 ml of phosphate buffer saline (PBS), pH 7.4, with 5% (v/v) calf serum, centrifuged at 500x**g**, re-suspended in 200 **µ**l of PBS, counted and immediately used. Cell viability, as determined by Trypan Blue exclusion, was typically never below 98%.

4.2. Respirometry

The oxygen consumption rate (OCR) was measured by high-resolution oxymetry (Oxygraph-2k, Oroboros Instruments or Oxygraph+ System, Hansatech Instruments Ltd) with Clark-type oxygen electrodes in a thermostatically controlled chamber equipped with a magnetic stirring device and a gas-tight stopper fitted with a narrow port for additions via Hamilton micro-syringes. Calibration of the instruments was made according to the manufacturer instructions. Measurements were carried out at 37 °C with about $2 \bullet 10^6$ HepG2 cells/ml suspended in 0.25 mM sucrose, 10 mM KH_2PO_4, 27 mM KCl, 40 mM Hepes, 1 mM $MgCl_2$, 0.5 mM EGTA, 0.1% BSA, pH 7.1. Inhibitory titrations of the respiratory activities were performed under resting conditions (OCR_{Rest}) or under uncoupled condition in the presence of 0.5 µM FCCP (OCR_{Unc}) by sequential additions of 0.5 **µ**l of freshly prepared differently concentrated solutions of KCN (in ddH_2O), myxothiazol (in ethanol), rotenone (in ethanol). Addition of the vehicle ethanol at the highest final volume attained following titration did not result in appreciable change in the OCR.

4.3. Metabolic flux control analysis.

The respiratory flux control coefficients ($C^{J}_{v,i}$) of the respiratory complexes I, III and IV were calculated by a non-linear regression analysis of the inhibitor-titration data set as developed in [25,26] and modified in [17,18] (fitting method). The derived non-linear equation correlating the percentage of the "global respiratory flux" to the inhibitor concentration [I] that we utilized:

$$J/J_0\ (\%) = 100\ E/(c^{J}_{v,i}\ (E_0\text{-}E) + E), \text{ with } E = -0.5\ (a - \sqrt{(a^2 + 4E_0K_D)}), \text{ and } a = [I] + K_D - E_0$$

depends on three parameters: K_D, which is the dissociation constant of the EI (enzyme-inhibitor) complex; E_0, which is the concentration of the active enzyme; $c^{J}_{v,i}$, which is the control coefficient of the inhibited enzymatic step (*i*). The K_Ds used were: 25 µM for the CIV-CN complex; 0.1 µM for the CIII-myxothiazol; 0.4 µM for the CI-rotenone complex. The content of cytochrome c oxidase-aa_3 (CIV) and bc_1 complex (CIII) was evaluated by the dithionite-reduced minus air-oxidized differential spectra of HepG2 cell lysate resulting in 4.8 ±0.5 pmol CIV/10^6 cells (n=5; $\Delta\varepsilon_{650-630nm}$=24 $mM^{-1}\ cm^{-1}$) and 2.1 ±0.4 pmol CIII/10^6 cells (n=5; $\Delta\varepsilon_{561-569\ nm}$=20 $mM^{-1}\ cm^{-1}$); thus values for E_0 of 0.0025 µM and 0.001 µM were imputed for CIV and CIII, respectively, at the prevailing experimental conditions (i.e. 2 x 10^6 HepG2 cells/ml). The amount of CI was assumed to be 0.8 pmol/10^6 cells (E_0=0.0004 µM) according to the relative respiratory chain complexes ratios computed in [27]. The parameters $c^{J}_{v,i}$ were estimated by best-fitting the inhibitory titration data set using the program GraFit 4.0.13 (Erithacus Software Ltd., Horley, Surrey, U.K.) enabling a tolerance range of ±50 % for the E_0s and K_Ds values. The accuracy of the fitting method was further tested for the CIV as in [18].

4.4. Fluorimetric measurement of $\Delta\Psi_m$.

3-5 x 10^6 HepG2 cells in 2 ml of the respiration assay buffer (0.25 M sucrose, 10 mM KH_2PO_4, 27 mM KCl, 40 mM Hepes, 1 mM $MgCl_2$, 0.5 mM EGTA, 0.1 % BSA, pH 7.1) were assayed by oxymetry and treated with increasing concentrations of the plasma membrane permeabilizer digitonine (Dig) to assess the minimum amount of Dig inhibiting the resting respiratory activity. The amount of Dig

Preprints (www.preprints.org) | NOT PEER-REVIEWED | Posted: 30 September 2023 doi:10.20944/preprints202309.2144.v1

chosen was for the fluorimetric analysis 20 µg/10^6 cells. For the fluorimetric measurement (by FP-6500, Jasco Analytical Instruments) 1.5-2.0 x 10^6 cells were preincubated for 20 min with the above reported concentration of Dig and pelleted at 1500-2000 rpm x 5 min. 2 ml of the buffer supplemented with 2 mM pyruvate plus 2 mM malate were placed in the fluorimeter cuvette (λ_{ex} 495 nm, λ_{em} 596 nm, medium gain) and four consecutive additions of 2.5 µM safranine O were injected, to calibrate the fluorescence signal; after than 1.5-2.0 x 10^6 cells (in 20 µL) were injected, causing progressive fluorescence quenching, followed after signal stabilization by addition of 0.4 µM FCCP causing full recovery of the safranine fluorescence. Estimation of the $\Delta\Psi_m$ was performed as in [18]. Briefly the following Nerst-derived equation was used:

$$\Delta\Psi m(mV)=60\cdot\log10[S]_{in}/[S]_{out}$$

with $[S]_{in}$ standing for intramitochondrial concentration of safranine, estimated from the fluorescence difference before and after the addition of FCCP [49] and $[S]_{out}$ standing for extramitochondrial concentration of safranine O, estimated from the fluorescence signal before the addition of FCCP. The value used for the intramitochondrial volume was 3 µl/10^6 HepG2 cells as computed in [18].

4.5. Blue native PAGE and Western blotting.

Mitochondrial-enriched fractions were obtained from HepG2 cells by differential centrifugation. Briefly, 10^8 cultured cells were harvested (by scraping) in 250 mM sucrose, 1 mM EDTA, 5 mM Hepes, 3 mM $MgCl_2$ (pH 7.4) supplemented with 10 µl/ml of protease inhibitors stock solution (SIGMA) and disrupted by tight teflon-glass homogenization; the homogenate was centrifuged at 1000 × *g* for 10 min and the resulting supernatant at 14,000 × *g* for 15 min. The resulting pellet was washed and finally re-suspended in a minimum volume of the same buffer supplemented with 0.6 g/g protein of dodecyl maltoside (DDM). Blue native-PAGE was performed in the presence of coomassie blu G250 as described in [27] in a 5–12% acrylamide gradient and a picture of the resulting gel digitally acquired and stored. Hence the gel was transferred to nitrocellulose membrane using an immersion electrophoretic transfer cell (Bio-Rad) at 40 V overnight at 4 °C and blotted with mouse anti-phospho serine (P-ser) (Becton Dickinson, 1:1000) and HPR-conjugated anti-mouse IgG (Thermo Scientific, 1:20,000) as primary and secondary Ab, respectively, according to standard Western blotting procedure, and visualized by chemiluminescence (Chemidoc Imaging System).

4.6. Statistical analysis.

Data are reported as the mean (± standard error mean, SEM) of at least three independent experiments as indicated in the legend to Figures. Data were compared by an unpaired Student's-*t*-test or, when necessary, by 2-way ANOVA followed by a post-hoc Bonferroni test. Differences were considered statistically significant with a p-values < 0.05. All analyses were performed using GraphPad Prism Software Version 5 (GraphPad Software Inc., San Diego, CA, USA).

Supplementary Materials: The following supporting information can be downloaded at the website of this paper posted on Preprints.org.

Author Contributions: Conceptualization, N.C.; methodology, N.C. and R.S.; software, G.C.; formal analysis, A.Q.N.; investigation, R.S., O.C., M.R., A.Q.N., F.T., A.L. and G.Q.; data curation, R.S and O.C.; writing—original draft preparation, N.C.; writing—review and editing, R.S. and A.Q.N.; visualization, N.C. and G.C.; supervision, N.C. and R.S.; funding acquisition, R.S., C.P. and N.C. All authors have read and agreed to the published version of the manuscript.

Funding: This research was financed by local funds from the University of Foggia, PRA-2014 and PRA-2022.

Conflicts of Interest: The authors declare no conflict of interest. The funders had no role in the design of the study; in the collection, analyses, or interpretation of data; in the writing of the manuscript; or in the decision to publish the results.

References

1. Efremov, R.G.; Baradaran, R.; Sazanov, L.A. The architecture of respiratory complex I. *Nature* **2010**, 27,465(7297).
2. Nicholls, D.G.; Ferguson, S.J. *Bioenergetics 3rd ed.* Academic Press, London, 2002.
3. Hackenbrock, C.R.; Chazotte, B.; Gupte, S.S. The random collision model and a critical assessment of diffusion and collision in mitochondrial electron transport. *J Bioenerg Biomembr* **1986**, 18(5), 331-68.
4. Schägger, H.; Pfeiffer, K. Supercomplexes in the respiratory chains of yeast and mammalian mitochondria. *EMBO J* **2000**, 19(8), 1777-83.
5. Lenaz, G.; Genova, M.L. Kinetics of integrated electron transfer in the mitochondrial respiratory chain: random collisions vs. solid state electron channeling. *Am J Physiol Cell Physiol* **2007**, 292(4), C1221-39.
6. Genova, M.L.; Lenaz, G. Functional role of mitochondrial respiratory supercomplexes. *Biochim Biophys Acta* **2014**, 1837(4), 427-43.
7. Acin-Perez, R.; Enriquez, J.A. The function of the respiratory supercomplexes: the plasticity model. *Biochim Biophys Acta* **2014**, 1837(4), 444-50.
8. Porras, C.A.; Bai, Y. Respiratory supercomplexes: plasticity and implications. *Front Biosci (Landmark Ed)* **2015**, 20(4), 621-34.
9. Cogliati, S.; Lorenzi, I.; Rigoni, G.; Caicci, F.; Soriano, M.E. Regulation of Mitochondrial Electron Transport Chain Assembly. *J Mol Biol*. **2018**, 430(24), 4849-4873.
10. Fernández-Vizarra, E.; López-Calcerrada, S.; Sierra-Magro, A.; Pérez-Pérez, R.; Formosa, L.E.; Hock, D.H.; Illescas, M.; Peñas, A.; Brischigliaro, M.; Ding, S.; Fearnley, I.M.; Tzoulis, C.; Pitceathly, R.D.S.; Arenas, J.; Martín, M.A.; Stroud, D.A.; Zeviani, M.; Ryan, M.T.; Ugalde, C. Two independent respiratory chains adapt OXPHOS performance to glycolytic switch. *Cell Metab* **2022**, 34(11), 1792-1808.
11. Kacser, H.; Burns, J.A. The control of flux. *Symp Soc Exp Biol* **1973**, 27, 65-104.
12. Heinrich, R.; Rapoport, T.A. A linear steady-state treatment of enzymatic chains. General properties, control and effector strength. *Eur J Biochem* **1974**, 42(1), 89-95.
13. Reder, C. Metabolic control theory: a structural approach. *J Theor Biol* **1988**, 135(2), 175-201.
14. Groen, A.K.; Wanders, R.J.; Westerhoff, H.V.; van der Meer, R.; Tager, J.M. Quantification of the contribution of various steps to the control of mitochondrial respiration. *J Biol Chem* **1982**, 257(6), 2754-7.
15. Tager, J.M.; Wanders, R.J.; Groen, A.K.; Kunz, W.; Bohnensack, R.; Küster, U.; Letko, G.; Böhme, G.; Duszynski, J.; Wojtczak, L. Control of mitochondrial respiration. *FEBS Lett* **1983**, 151(1), 1-9.
16. Brown, G.C. Control of respiration and ATP synthesis in mammalian mitochondria and cells. *Biochem J* **1992**, 284 (Pt 1)(Pt 1), 1-13.1982.
17. Piccoli, C.; Scrima, R.; Boffoli, D.; Capitanio, N. Control by cytochrome c oxidase of the cellular oxidative phosphorylation system depends on the mitochondrial energy state. *Biochem. J* **2006**, 396573–583.
18. Quarato, G.; Piccoli, C.; Scrima, R.; Capitanio, N. Variation of flux control coefficient of cytochrome c oxidase and of the other respiratory chain complexes at different values of protonmotive force occurs by a threshold mechanism. *Biochim Biophys Acta* **2011**,1807(9), 1114-24.
19. Stram, A.R.; Payne, R.M. Post-translational modifications in mitochondria: protein signaling in the powerhouse. *Cell Mol Life Sci* **2016**, 73(21), 4063-73.
20. Zhao, X.; León, I.R.; Bak, S.; Mogensen, M.; Wrzesinski, K.; Højlund, K.; Jensen, O.N. Phosphoproteome analysis of functional mitochondria isolated from resting human muscle reveals extensive phosphorylation of inner membrane protein complexes and enzymes. *Mol Cell Proteomics* **2011**, 10(1), M110.000299.
21. Castellanos, E.; Lanning, N.J. Phosphorylation of OXPHOS Machinery Subunits: Functional Implications in Cell Biology and Disease. *Yale J Biol Med* **2019**, 92(3), 523-531.
22. Niemi, N.M.; Pagliarini, D.J. The extensive and functionally uncharacterized mitochondrial phosphoproteome. *J Biol Chem* **2021**, 297(1), 100880.
23. Thomson, M. Evidence of undiscovered cell regulatory mechanisms: phosphoproteins and protein kinases in mitochondria. *Cell Mol Life Sci* **2002**, 59(2), 213–219.
24. Horbinski, C.; Chu, C.T. Kinase signaling cascades in the mitochondrion: a matter of life or death. *Free Radic Biol Med* **2005**, 38(1), 2–11.
25. Gellerich, F.N.; Kunz, W.S.; Bohnensack, R. Estimation of flux control coefficients from inhibitor titrations by non-linear regression. *FEBS Lett* 1990, 274, 167–170.
26. Small, J.R. Flux control coefficients determined by inhibitor titration: the design and analysis of experiments to minimize errors. *Biochem. J* 1993, 296, 423–433.
27. Schägger, H.; Pfeiffer, K. The ratio of oxidative phosphorylation complexes I-V in bovine heart mitochondria and the composition of respiratory chain supercomplexes. *J Biol Chem* **2001**, 276(41), 37861-7.
28. Torres-Quesada, O.; Mayrhofer, J.E.; Stefan, E. The many faces of compartmentalized PKA signalosomes. *Cell Signal* **2017**, 37, 1-11.
29. Ould Amer, Y.; Hebert-Chatelain, E. Mitochondrial cAMP-PKA signaling: What do we really know? *Biochim Biophys Acta Bioenerg* **2018**, 1859(9), 868-877.
30. Valsecchi, F.; Konrad, C.; Manfredi, G. Role of soluble adenylyl cyclase in mitochondria. *Biochim Biophys Acta* **2014**,1842(12 Pt B), 2555-60.

31. Bitterman, J.L.; Ramos-Espiritu, L.; Diaz, A.; Levin, L.R.; Buck, J. Pharmacological distinction between soluble and transmembrane adenylyl cyclases. *J Pharmacol Exp Ther* **2013**, 347(3), 589-98.
32. Wu, M.; Gu, J.; Guo, R.; Huang, Y.; Yang, M. Structure of Mammalian Respiratory Supercomplex $I_1III_2IV_1$. *Cell* **2016,** 167(6),1598-1609.
33. Milenkovic, D.; Misic J.; Hevler, J. F.; Molinie´,T.; Chung, I.; Atanassov, I.; Li, X.; Filograna, R.; Mesaros, A.; Mourier, A.; Heck, A.J.R.; Hirst, J.; Larsson, N.G. Preserved respiratory chain capacity and physiology in mice with profoundly reduced levels of mitochondrial respirasomes. *Cell Metabolism* **2023**, 35, 1–15.
34. Guo, R.; Zong, S.; Wu, M.; Gu, J.; Yang, M. Architecture of Human Mitochondrial Respiratory Megacomplex $I_2III_2IV_2$. *Cell* **2017**, 170(6), 1247-1257.e12.
35. Fernández-Vizarra, E.; Ugalde, C. Cooperative assembly of the mitochondrial respiratory chain. *Trends Biochem Sci* **2022**, 47(12), 999-1008.
36. Maranzana, E.; Barbero, G.; Falasca, A.I.; Lenaz, G.; Genova, M.L. Mitochondrial Respiratory Supercomplex Association Limits Production of Reactive Oxygen Species from Complex I. *Antioxid. Redox Signal* **2013**, 19, 1469–1480.
37. Toth, A.; Meyrat, A.; Stoldt, S.; Santiago, R.; Wenzel, D.; Jakobs, S.; von Ballmoos, C.; Ott, M. Kinetic coupling of the respiratory chain with ATP synthase, but not proton gradients, drives ATP production in cristae membranes. *Proc Natl Acad Sci U S A* **2020**, 117(5), 2412-2421.
38. Lobo-Jarne, T.; Ugalde, C. Respiratory chain supercomplexes: Structures, function and biogenesis. *Semin Cell Dev Biol* **2018**, 76, 179-190.
39. Zhang, K.; Chen, L.; Wang, B.; Chen, D.; Ye, X.; Han, X.; Fang, Q.; Yu, C.; Wu, J.; Guo, S.; Chen, L.; Shi, Y.; Wang, L.; Cheng, H.; Li, H.; Shen, L.; Zhao, Q.; Jin, L.; Lyu, J.; Fang, H. Mitochondrial supercomplex assembly regulates metabolic features and glutamine dependency in mammalian cells. *Theranostics* **2023**, 13(10), 3165-3187.
40. Villani, G.; Attardi, G. In vivo measurements of respiration control by cytochrome c oxidase and in situ analysis of oxidative phosphorylation. *Methods Cell Biol* **2001**, 65, 119-31.
41. Jakobsen, E.; Andersen, J.V.; Christensen, S.K.; Siamka, O.; Larsen, M.R.; Waagepetersen, H.S.; Aldana, B.I.; Bak, L.K. Pharmacological inhibition of mitochondrial soluble adenylyl cyclase in astrocytes causes activation of AMP-activated protein kinase and induces breakdown of glycogen. *Glia* **2021**, 69(12), 2828-2844.
42. Scacco, S.; Vergari, R.; Scarpulla, R.C.; Technikova-Dobrova, Z.; Sardanelli, A.; Lambo, R.; Lorusso, V.; Papa, S. cAMP-dependent phosphorylation of the nuclear encoded 18-kDa (IP) subunit of respiratory complex I and activation of the complex in serum-starved mouse fibroblast cultures. *J Biol Chem* **2000,** 275(23), 17578-82.
43. Piccoli, C.; Scacco, S.; Bellomo, F.; Signorile, A.; Iuso, A.; Boffoli, D.; Scrima, R.; Capitanio, N.; Papa, S. cAMP controls oxygen metabolism in mammalian cells. *FEBS Lett* **2006**, 580(18), 4539-43.
44. Signorile, A.; Pacelli, C.; Palese, L.L.; Santeramo, A.; Roca, E.; Cocco, T.; De Rasmo, D. cAMP/PKA Signaling Modulates Mitochondrial Supercomplex Organization. *Int J Mol Sci* **2022**, 23(17), 9655.
45. Kasimova, M.A.; Lindahl, E.; Delemotte, L. Determining the molecular basis of voltage sensitivity in membrane proteins. *J Gen Physiol* **2018**, 150(10), 1444-1458.
46. Catacuzzeno, L.; Conti, F.; Franciolini, F. Fifty years of gating currents and channel gating. *J Gen Physiol* **2023**, 155(8), e202313380.
47. Bezanilla, F. How membrane proteins sense voltage. *Nat Rev Mol Cell Biol* **2008**, 9(4), 323-32.
48. Zhang, X.C.; Li, H. Interplay between the electrostatic membrane potential and conformational changes in membrane proteins. *Protein Sci* **2019,** 28(3), 502-512.
49. Akerman, K.E.; Wikström, M.K. Safranine as a probe of the mitochondrial membrane potential. *FEBS Lett* **1976**, 68(2):191-7.